Stimulated orientational and thermal scatterings and self-starting optical phase conjugation with nematic liquid crystals

I. C. Khoo and Y. Liang
Department of Electrical Engineering, Pennsylvania State University, University Park, Pennsylvania 16802
(Received 23 February 2000)

A quantitative theory and experimental results on self-starting optical phase conjugation, using stimulated orientational and thermal scattering in nematic liquid crystal films, are presented. The coupled wave-material equations for the laser-induced refractive index changes, grating formation, and coherent wave mixing effects are developed. Analytical solutions are obtained for the case of negligible pump depletion, and numerical solutions for various input and generated signals, taking losses into account, are obtained. Experimentally, we demonstrate the feasibility of realizing these stimulated scattering and phase conjugation processes in thin (200 μm) nematic liquid crystal with a milliwatt-power cw laser. Theoretical estimates for various gain constants and threshold intensities, and their dependence on various physical parameters, are found to be in good agreement with experimental observations.

PACS number(s): 61.30.Gd, 42.79.Kr, 42.70.Mp, 42.65.Hw

I. INTRODUCTION

Self-starting optical phase conjugation (SSOPC), in which a single incident laser beam generates its phase conjugated replica via some optical wave mixing effect in a nonlinear optical material, is a fundamentally interesting and practically useful process [1]. Usually, the signal originates as some noise scattered from the pump beam, e.g., from scattering centers in a crystal, spontaneous Brillouin or Raman scattering, etc. This noise signal interacts coherently with the pump beam, and grows into a strong coherent signal. This phenomenon is commonly observed in stimulated Brillouin scattering involving high-power pulsed lasers [1,2], and in photorefractive materials with low-power cw lasers [3,4]. A self-pumped phase conjugation effect was also observed in resonant media, using frequency-shifted signal and pump fields [5], or a degenerate four-wave mixing process [6].

In two previous short papers [7,8], we reported the observation of self-pumped optical phase conjugation from nematic liquid crystal films, using low-power cw visible lasers. Similar SSOPC effects were also reported by Antipov and co-workers [9]. The fundamental mechanisms involved are the refractive index changes caused by thermal indexing or the nematic axis orientational effect. A related study [10] demonstrated the feasibility of SSOPC, and Khoo *et al.* [11] demonstrated beam amplification by wave mixing in the infrared regime (a 10.6-μm CO_2 laser) using the broadband (near UV to-far-infrared region) birefringence and thermal index coefficients [12] of nenatic liquid crystals.

In this paper, we present a comprehensive account of the underlying theories for the phenomena, and experimental verification of various parametric dependences. Following this introduction, coupled wave equations for input and generated optical waves, and material equations describing the laser induced refractive index changes in the nematic films, are formulated in Sec. II. Both stimulated thermal and orientational scattering processes in the nematic film can be cast into a general diffusive equation. In Sec. III, steady state solutions of coupled wave equations are solved analytically under the no-pump depletion limit, allowing us to gain physical insights into the oscillation conditions and various dynamical and parametric dependencies of the stimulated scattering and self-starting optical phase conjugation processes. In Sec. IV, we discuss the special case of stimulated scatterings involving only an incident pump wave and its scattered noise. This is followed in Sec. V by a discussion of hitherto unreported experimental results of stimulated orientational scattering (SOS), simulated thermal scattering (STS), and SSOPC in the context of the theoretical formalism presented, and concluding remarks.

II. THEORETICAL FORMALISMS

Consider the interaction geometry as depicted in Fig. 1(a). An incident laser traverses the nematic liquid crystal (NLC) film twice, once as an incident field $\mathbf{E}_1$ (along $\mathbf{k}_1$ direction) and then, on reflection from the optical feedback system behind the sample, as a reflected field $\mathbf{E}_2$ (along the $\mathbf{k}_2$ direction). $\mathbf{E}_1$ and $\mathbf{E}_2$ are not necessarily coherent with respect to each other. The incident beam generates a noise source field E_3 (along $\mathbf{k}_3$) that is coherent with respect to $\mathbf{E}_1$. Accordingly, $\mathbf{E}_1$ and $\mathbf{E}_3$ can interfere with each other and produce an index grating. Similarly, the reflected field $\mathbf{E}_2$ will interfere with its coherent noise $\mathbf{E}_4$ and will produce an index grating.

In general, the scattered noises $\mathbf{E}_3$ and $\mathbf{E}_4$ contain various temporal- and spatial-frequency components, cf. Fig. 1(b). For a given crossing angle between the incident and reflected beams in the experiment, only the scattered-noise components ($\mathbf{k}_3=-\mathbf{k}_2$ and $\mathbf{k}_4=-\mathbf{k}_1$) that obey the phase-matching condition depicted in Fig. 1(c) are able to share a common grating ($\mathbf{q}=\mathbf{k}_1-\mathbf{k}_3=\mathbf{k}_2-\mathbf{k}_4$) and contribute to each other's growth. In this circumstance, $\mathbf{E}_3$ and $\mathbf{E}_4$ also serve as a feedback to one another, via reflections by the external mirrors. This particular set of phase-conjugated signals $\mathbf{E}_3$ and $\mathbf{E}_4$ (along $\mathbf{k}_4$ and $\mathbf{k}_3$ directions respectively) has an advantage over other noise components in experiencing gain, and grow into coherent beams.

In STS, in which the director axis is considered fixed, the

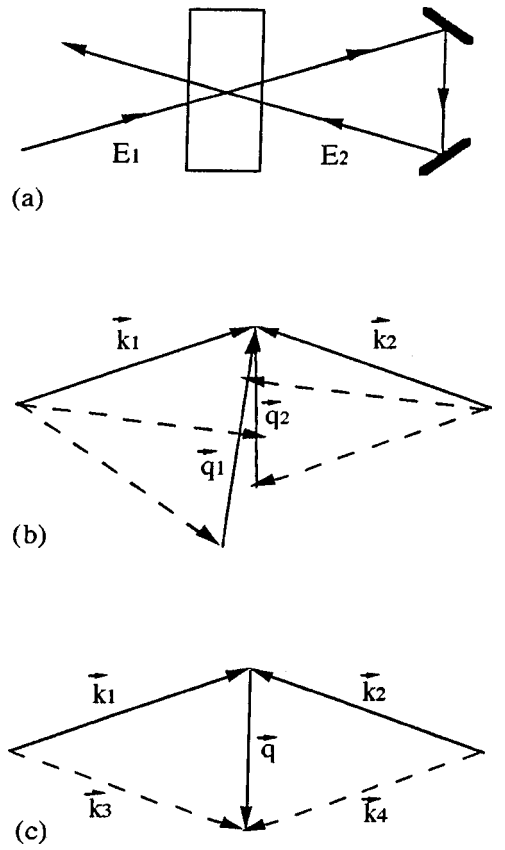

FIG. 1. Ring-mirror cavity configuration for generation of a self-pumped phase conjugation. (a) Experimental setup. (b) Wave vectors of the input beams and the scattering noises; dashed lines represent the scattering noise, and solid lines are input beams. (c) Single grating for phase-matched interaction.

incident and generated noises $\mathbf{E}_1$ and $\mathbf{E}_3$ are copolarized. On the other hand, in SOS (cf. Fig. 2), the signal wave $\mathbf{E}_3$ is orthogonally polarized with respect to $\mathbf{E}_1$ due to the optically induced director axis reorientation. In this case, in order to fulfill the wave-vector matching condition and take advantage of the feedback of the external mirrors, the reflected beam $\mathbf{E}_2$ has to be orthogonally polarized to that of the input beam $\mathbf{E}_1$ [cf. Fig. 1(d)]

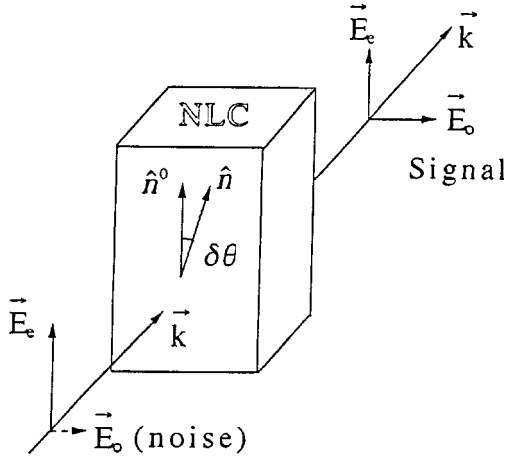

FIG. 2. Generation of stimulated orientational scattering in nematic liquid crystals.

A. Coupled-wave equations and boundary conditions

Inside the nematic film, two pairs of coherent waves ($\mathbf{E}_1$ and $\mathbf{E}_3$) and ($\mathbf{E}_2$ and $\mathbf{E}_4$) give rise to two sets of intensity gratings. The optical electric fields and intensity are therefore given by,

$$E_j(r,t)=E_j(z,t)e^{i(k_j r-\omega_j t)} \quad (j=1,2,3,\text{and } 4) \tag{1}$$

and

$$I=I_0+(E_1^*E_3+E_2^*E_4)e^{i(q\cdot r-\Omega t)}+\text{c.c.}, \tag{2}$$

respectively, where

$$q=k_3-k_1=k_4-k_2, \tag{3}$$

$$\Omega=\omega_3-\omega_1=\omega_4-\omega_2, \tag{4}$$

$$I_0=|E_1|^2+|E_2|^2+|E_3|^2+|E_4|^2. \tag{5}$$

The optically induced refractive index change in the nematic film can similarly be written as

$$\delta n=\delta n_0+\delta n_q e^{i(q\cdot r-\Omega t)}+\delta n_q^* e^{-i(q\cdot r-\Omega t)}. \tag{6}$$

The coupled-wave equations resulting from the index gratings are therefore given by [13,14]

$$\frac{dE_1}{dz}=i\frac{n_0\omega^2}{k_{1z}c^2}\delta n_q^* E_3, \tag{7}$$

$$\frac{dE_2}{dz}=i\frac{n_0\omega^2}{k_{2z}c^2}\delta n_q^* E_4, \tag{8}$$

$$\frac{dE_3}{dz}=i\frac{n_0\omega^2}{k_{3z}c^2}\delta n_q E_1, \tag{9}$$

$$\frac{dE_4}{dz}=i\frac{n_0\omega^2}{k_{4z}c^2}\delta n_q E_2. \tag{10}$$

For simplicity of illustration, we have written these equations in scalar form, bearing in mind that, in the thermal effect, all waves are copolarized, whereas in an orientational scattering $\mathbf{E}_1$ and $\mathbf{E}_2$ are orthogonally polarized to their respective scattered components $\mathbf{E}_3$ and $\mathbf{E}_4$ [13,14].

The initial conditions for these optical waves are

$$E_1(0)=E_0, \quad E_2(1)=rE_1(1), \quad E_4(1)=rE_3(1), \tag{11}$$

where E_0 is the amplitude of the incident beam, and r is the amplitude reflectivity of the external mirrors. The scattered noise source E_3 is related to the input E_1 by a spontaneous scattering coefficient η_{ss}:

$$\eta_{ss}=\frac{E_3(0)}{E_1(0)}. \tag{12}$$

B. Material equation and solutions

Although the two mechanisms for optical nonlinearities in NLCs, namely, thermal effect and director axis reorientation, are quite different, the resulting index changes by both

mechanisms satisfy the same form of the diffusion equation, under the one-elastic constant approximation [12–14]

$$\frac{d\,\delta n_q}{dt}+\frac{\delta n_q}{\tau}=\chi(E_1^*E_3+E_2^*E_4), \tag{13}$$

where

$$\frac{1}{\tau}=\frac{1}{\tau_q}-i\Omega, \tag{14a}$$

and τ_q is the grating relaxation time. For the director reorientation effect, $\tau_q=\tau_R=\eta/Kq^2$, and

$$\chi=\chi_R=\frac{\varepsilon_a^2}{4n_0^2c\,\eta}. \tag{14b}$$

where ε_a is the optical anisotropy of the NLC, and K and η are the appropriate elastic constant and viscosity coefficient, respectively. For the thermal effect, $\tau_q=\tau_T=1/Dq^2$, and the coupling coefficient is

$$\chi_T=\frac{\alpha\left(\frac{dn}{dT}\right)}{\rho c_p}\left(\frac{n_0c}{8\pi}\right). \tag{14c}$$

The set of coupled optical wave and material equations (7)–(13) can be solved numerically to describe the complete electrodynamics of the various underlying nonlinear optical processes. To gain physical insights, and obtain threshold conditions and parametric dependence, the steady state solutions of these equations will be sufficient and instructive. In this case, we have

$$\delta n_q=\tau_q\chi\frac{(E_1^*E_3+E_2^*E_4)}{1-i\Omega\tau_q}, \tag{15}$$

$$\frac{dE_1}{dz}=-\gamma^*\frac{(E_1E_3^*+E_2E_4^*)E_3}{I_0}, \tag{16}$$

$$\frac{dE_2}{dz}=\gamma^*\frac{(E_1E_3^*+E_2E_4^*)E_4}{I_0}, \tag{17}$$

$$\frac{dE_3}{dz}=\gamma\frac{(E_1^*E_3+E_2^*E_4)E_1}{I_0}, \tag{18}$$

$$\frac{dE_4}{dz}=-\gamma\frac{(E_1^*E_3+E_2^*E_4)E_2}{I_0}, \tag{19}$$

where we have define a complex coupling coefficient:

$$\gamma=i\frac{\omega\tau_q\chi I_0}{c\cos\frac{\Theta}{2}}\frac{1}{1-i\Omega\tau_q},\quad \gamma=|\gamma|e^{i\phi}=g+i\kappa. \tag{20}$$

Also, we have used $k_{1z}=k_{3z}=-k_{2z}=-k_{4z}=(n_0\omega/c)\cos(\Theta/2)$. If we write $E_j=|E_j|e^{i\psi j}$, where ψ_j are phases of the complex optical electric field amplitude E_j, the coupled equations for the intensities $I_j=|E_j|^2$ can be derived from Eqs. (16)–(19) as

$$\frac{dI_1}{dz}=-\frac{2}{I_0}\{gI_1I_3+|\gamma|\sqrt{I_1I_2I_3I_4}\times\cos[-\phi-(\psi_1-\psi_3)+(\psi_2-\psi_4)], \tag{21}$$

$$\frac{dI_2}{dz}=\frac{2}{I_0}\{gI_2I_4+|\gamma|\sqrt{I_1I_2I_3I_4}\times\cos[-\phi+(\psi_1-\psi_3)-(\psi_2-\psi_4)], \tag{22}$$

$$\frac{dI_3}{dz}=\frac{2}{I_0}\{gI_1I_3+|\gamma|\sqrt{I_1I_2I_3I_4}\times\cos[\phi+(\psi_1-\psi_3)-(\psi_2-\psi_4)]\}, \tag{23}$$

$$\frac{dI_4}{dz}=-\frac{2}{I_0}\{gI_2I_4+|\gamma|\sqrt{I_1I_2I_3I_4}\times\cos[\phi-(\psi_1-\psi_3)+(\psi_2-\psi_4)], \tag{24}$$

and a set of similar equations for the phases ψ's.

An important point to note is that, since E_3 and E_4 are coherently scattered from E_1 and E_2 respectively, the pairs (E_1 and E_3), and (E_2 and E_4) should be in phase. This means $\psi_1-\psi_3=$const and $\psi_2-\psi_4=$const, respectively. Therefore, although the phases of E_1 and E_2 (E_3 and E_4) are not related, the phase factor appearing in Eqs. (21)–(24) above, namely, $(\psi_1-\psi_3)-(\psi_2-\psi_4)$, is a constant. For convenience, we can set this constant to be 0, i.e., $(\psi_1-\psi_3)-(\psi_2-\psi_4)=0$. This condition simplifies the solution of the complex coupled wave equation considerably.

III. SSOPC SOLUTIONS AND DISCUSSIONS

In general, a complete solution of the coupled complex electric field requires some numerical techniques. However, if we apply the assumptions of small signals, i.e., I_3, $I_4\ll I_1$, I_2, and thus no pump depletion, i.e., $I_1=I_0$ and $I_2=r^2I_0$, analytical solutions can be obtained that will clearly illustrate the essential physics. Also, one could obtain a very good theoretical estimate of various threshold conditions and dynamical dependences on various optical, material and physical parameters.

Since the phase factors appearing in the coupled equations are constant, we need to consider the amplitude of the optical wave. Accordingly, we have

$$\frac{d|E_3|}{dz}=g_{\rm eff}(|E_3|+r_{\rm eff}|E_4|)-\frac{\alpha}{2}|E_3|, \tag{25a}$$

$$\frac{d|E_4|}{dz}=-g_{\rm eff}r_{ef}(|E_3|+r_{\rm eff}|E_4|)+\frac{\alpha}{2}|E_4|, \tag{25b}$$

where we have introduced the phenomenological loss terms on the right-hand side of the equations to simulate losses dues to scattering and absorption, i.e., the total loss $\alpha=\alpha_a+\alpha_s$, where α_a is the absorption and α_s the scattering loss, respectively. In these equations, we have also replaced g by $g_{\rm eff}$ and r by $r_{\rm eff}$ to account for the fact that due to such losses, the effective value of the pump beam in the medium is slightly different from I_0. One approximate form for $g_{\rm eff}$

and r_{eff} could be obtained if we employ the average values for the pump beams I_1 and I_2 as follows:

$$\overline{I_1}=\frac{1}{l}\int_0^l I_1(z)dz=I_o\frac{1-e^{-\alpha l}}{\alpha l},$$

$$\overline{I_2}=\frac{1}{l}\int_l^0 I_2(z)d(-z)=I_o r^2 e^{-\alpha l}\frac{1-e^{-\alpha l}}{\alpha l},$$

$$g_{\text{eff}}=g\frac{1-e^{-\alpha l}}{\alpha l},\quad r_{\text{eff}}=re^{-\alpha l/2}. \tag{26}$$

As noted above, these approximations allow us to obtain analytical solutions without loss of physics. They are of course not necessary if the above equations are to be solved by numerical techniques.

A. Solution of the coupled intensity equations—no loss

Consider the case of $\alpha=0$. We have

$$|E_3(z)|=|\eta_{ss}E_0|\frac{e^{(1-r^2)gz}-\dfrac{2r^2}{1+r^2}e^{(1-r^2)gl}}{1-\dfrac{2r^2}{1+r^2}e^{(1-r^2)gl}}, \tag{27a}$$

$$|E_4(z)|=r|\eta_{ss}E_0|\frac{\dfrac{2}{1+r^2}e^{(1-r^2)gl}-e^{(1-r^2)gz}}{1-\dfrac{2r^2}{1+r^2}e^{(1-r^2)gl}}. \tag{27b}$$

At the output boundaries $z=1$ and 0 of interest, the signals are

$$|E_3(l)|=|\eta_{ss}E_0|\frac{\dfrac{1-r^2}{1+r^2}e^{(1-r^2)gl}}{1-\dfrac{2r^2}{1+r^2}e^{(1-r^2)gl}}, \tag{28a}$$

$$|E_4(0)|=\tau|\eta_{ss}E_0|\frac{\dfrac{2}{1+r^2}e^{(1-r^2)gl}-1}{1-\dfrac{2r^2}{1+r^2}e^{(1-r^2)gl}}. \tag{28b}$$

The amplification of the output signal $I_4(0)$ over the noise level $I_3(0)=|\eta_{ss}E_0|^2$ is a function of the gain parameter gl and reflectivity r^2. The dependence of the phase-conjugated signal reflectivity $E_4(0)/E_3(0)$ [note $E_3(0)=\eta_{ss}E_1(0)$] on the gain constant gl is shown in Fig. 3(a). Note that the signal reflectivity diverges at some finite values of gl, signifying the possibility of self-oscillations.

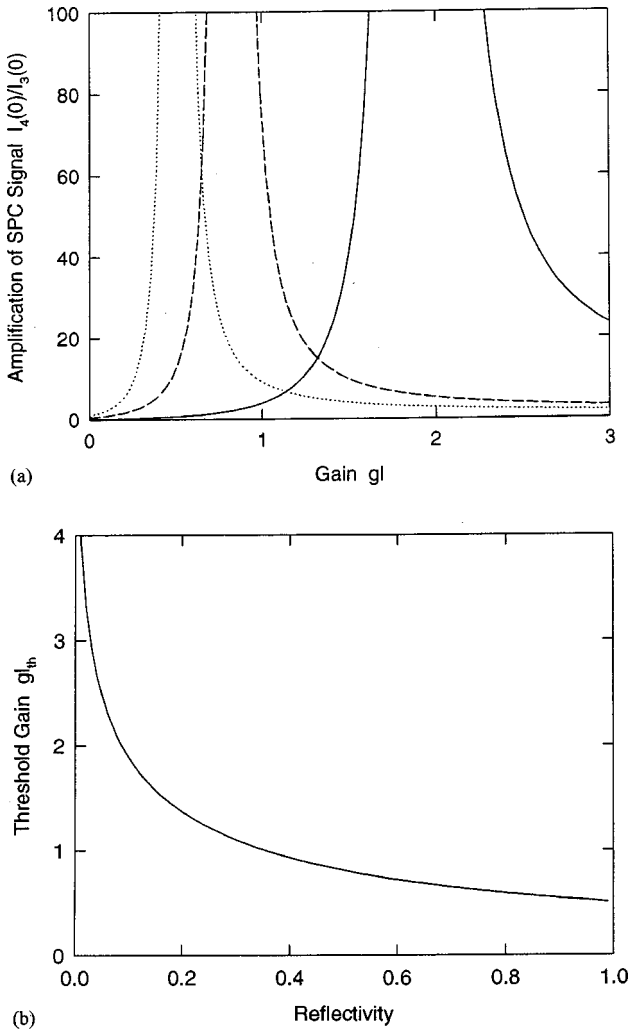

FIG. 3. (a) Amplification of the SPC signal as a function of the gain factor, when the reflectivity is $r^2=0.99$ (dots), $r^2=0.5$ (dashed line), and $r^2=0.1$ (solid line). (b) Threshold gain factor for self-oscillation as a function of the feedback.

The self-oscillation condition can be derived directly from the above solutions by setting the denominator to zero. This yields

$$1-\frac{2r^2}{1+r^2}e^{(1-r^2)gl}=0\rightarrow(gl)_{\text{th}}=\frac{1}{1-r^2}\ln\frac{1+r^2}{2r^2}. \tag{29}$$

The dependence of the threshold gain constant $(gl)_{\text{th}}$ on the feedback reflectivity r is shown in Fig. 3(b); the threshold decreases monotonically as the reflectivity increases. Note that for $r=0$, i.e., there is no feedback from the external mirrors, the above solutions reduce to the case of stimulated scattering involving the incident pump beam and its noise. In this process, the signal intensity grows exponentially with the coupling strength gl. We will discuss more details of these processes in Sec. IV.

B. Solution with consideration of loss

If $\alpha\neq 0$, the solutions for E_3 and E_4, after some straightforward but tedious algebra, are obtained as follows:

$$|E_3(z)| = |\eta_{ss}E_0| e^{\lambda_1 z} \frac{\left[\lambda_1 - g_{eff}(1+r_{eff}^2) + \frac{\alpha}{2}\right]\sinh\lambda_2(l-z) + \lambda_2\cosh\lambda_2(l-z)}{\left[\lambda_1 - g_{eff}(1+r_{eff}^2) + \frac{\alpha}{2}\right]\sinh\lambda_2 l + \lambda_2\cosh\lambda_2 l}, \tag{30a}$$

$$|E_4(z)| = \frac{|\eta_{ss}E_0| e^{\lambda_1 s}}{\left[\lambda_1 - g_{eff}(1+r_{eff}^2) + \frac{\alpha}{2}\right]\sinh\lambda_2 l + \lambda_2\cosh\lambda_2 l} \frac{1}{g_{eff}r_{eff}} \left\{\left[\left(\lambda_1 - g_{eff} + \frac{\alpha}{2}\right)\left(\lambda_1 - g_{eff}(1+r_{eff}^2) + \frac{\alpha}{2}\right) - \lambda_2^2\right]\right.$$

$$\left. \times \sinh\lambda_2(l-z) + \lambda_2 g_{eff} r_{eff}^2 \cosh\lambda_2(l-z)\right\}, \tag{30b}$$

where

$$\lambda_1 = \tfrac{1}{2} g_{eff}(1 - r_{eff}^2) \tag{31a}$$

$$\lambda_2 = \tfrac{1}{2}\sqrt{[g_{eff}(1+r_{eff}^2) - \alpha]^2 - 4g_{eff}^2 r_{eff}^2} = \tfrac{1}{2}\sqrt{[g_{eff}(1+r_{eff}^2) - \alpha][g_{eff}(1-r_{eff})^2 - \alpha]}. \tag{31b}$$

At the output boundaries $z=1$ and 0 of interest, we have

$$|E_3(l)| = \frac{|\eta_{ss}E_0|\lambda_2 e^{\lambda_1 z}}{\left[\lambda_1 - g_{eff}(1+r_{eff}^2) + \frac{\alpha}{2}\right]\sinh\lambda_2 1 + \lambda_2\cosh\lambda_2 l}, \tag{32a}$$

$$|E_4(0)| = \frac{|\eta_{ss}E_0|}{g_{eff}r_{eff}} \frac{\left[\left(\lambda_1 - g_{eff} + \frac{\alpha}{2}\right)\left(\lambda_1 - g_{eff}(1+r_{eff}^2) + \frac{\alpha}{2}\right) - \lambda_2^2\right]\sinh\lambda_2 l + \lambda_2 g_{eff} r_{eff}^2 \cosh\lambda_2 l}{\left[\lambda_1 - g_{eff}(1+r_{eff}^2) + \frac{\alpha}{2}\right]\sinh\lambda_2 1 + \lambda_2\cosh\lambda_2 l}. \tag{32b}$$

With Eq. (32b), we can study how the phase-conjugated signal depends on the pump intensity I_o, the spontaneous scattering ration η_{ss} the feedback r_{eff}^2, the loss α, and other optical and material parameters involved in the SOS- and STS-initiated SSOPC processes.

In particular, the self-oscillation condition is obtained by setting the denominator of the above expressions to zero:

$$\left[\lambda_1 - g_{eff}(1+r_{eff}^2) + \frac{\alpha}{2}\right]\sinh\lambda_2 1 + \lambda_2\cosh\lambda_2 l = 0. \tag{33}$$

Since the coupling strength g_{eff}^1 is proportional to the input pump intensity I_o according to Eq. (20), the self-oscillation condition defined by Eq. (33) determines a threshold pump intensity I_{th}. Figures 4(a) and 4(b) shows the dependence of I_{th} on the feedback reflectivity r_{eff}^2 and medium loss α, calculated using typical parameters used in *stimulated orientational* scattering (c.f. Sec. IV) section. In general, I_{th} decreases as r_{eff}^2 increases, and increases as α increases, as expected.

In the case of SSOPC by STS, the coupling coefficient is dependent on the absorption constant α_a, so the dependence of the threshold I_{th} on α_a is quite different from SOS-initiated SSOPC. The nonlinear coupling constant χ due to thermal effect is proportional to the light absorption as shown in Eq. (14c), so that a higher absorption helps to lower the threshold for self-oscillation. On the other hand, a higher absorption means larger loss of the signal and pump, which implies a higher oscillation threshold value. Therefore, an optimum value of α should exist for the experiment. Figure 5 shows the relationship between I_{th} and the light absorption constant α_a, for various values of the feedback reflectivity in which the parameters of NLC's for the STS effect are used. In each case, there is an optimum value of α_a where the threshold I_{th} is a minimum.

IV. STIMULATED ORIENTATIONAL AND THERMAL SCATTERINGS

Since the underlying mechanisms for the SSOPC's under study here are the stimulated orientational and thermal scatterings, it is instructive to examine these two fundamental processes separately, and gain more insights. As remarked above, STS and SOS correspond to special cases of SSOPC without feedback ($r=0$). The basic equations are given by Eqs. (16) and (17), modified to include the phenomenological loss term.

A. Stimulated orientational scattering (SOS)

In the case of SOS, the coupled wave equations for the incident E_0 and its coherent scattered noise component E_e, deduced from Eqs. (16) and (17), become

$$E_0(z) = E_0(0)e^{-(\alpha/2)z}, \tag{34a}$$

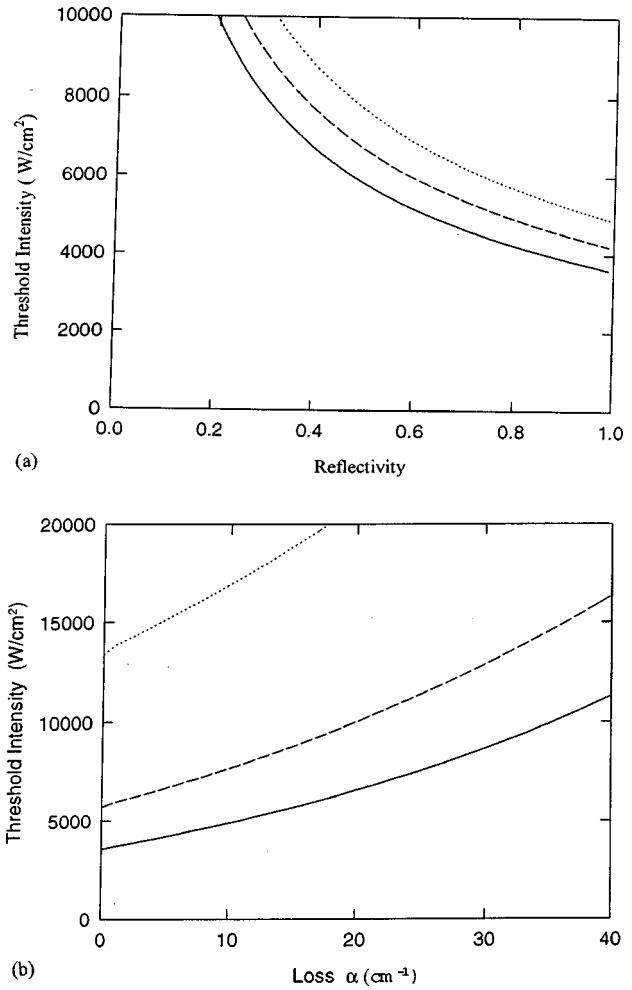

FIG. 4. (a) Dependence of the threshold pump intensity threshold for self-oscillation on the feedback, when the loss $\alpha=0$ (solid line), $\alpha=5$ cm (dashed line), and $\alpha=10$/cm (dots). (b) Dependence of the threshold pump intensity for self-oscillation of the SPC signal on the light loss, when the reflectivity of the mirrors are $r^2=0.99$ (solid line), $r^2=0.5$ (dashed line), and $r^2=0.1$ (dots).

$$\frac{dE_e}{dz}=\gamma_R e^{-\alpha z}E_e-\frac{\alpha}{2}E_e, \tag{34b}$$

$$\gamma_R=i\frac{\omega\varepsilon_a{}^2|E_0|^2}{32\pi n_\parallel cKq^2}\frac{1+i\Omega\tau_R}{1+(\Omega\tau_R)^2}=g_R+i\kappa_R, \tag{35}$$

where we have included the phenomenological loss term $-\alpha E_e/2$, and used relations (14b) and (20) to define the coupling constant γ_R. From Eq. (34b), the intensity of $I_e(1)$ at the output plane $z=1$ is given by $I_e(l)=I_e(0)e^{[2g_R f(\alpha l)-\alpha]l}$,
where

$$g_R=\mathrm{Re}(\gamma_R)=\frac{\omega\varepsilon_a{}^2|E_0|^2}{64\pi n_\parallel cKq^2}\frac{-2\Omega\tau_R}{1+(\Omega\tau_R)^2}$$

$$=\frac{\omega\varepsilon_a{}^2|E_0|^2}{8c^2 n_\parallel n_\perp Kq^2}\frac{-2\Omega\tau_R}{1+(\Omega\tau_R)^2}, \tag{36}$$

and $f(\alpha z)=(1-e^{-\alpha z})/\alpha z$. Equation (36) shows that the gain is positive if $\Omega(\omega_3<\omega_1)<0$, i.e., only the Stokes wave

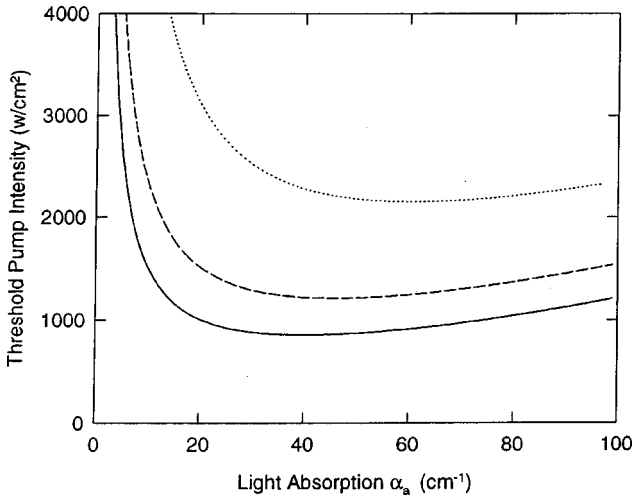

FIG. 5. Dependence of the threshold pump intensity for SSOPC on the light absorption of the dye-doped NLC, when the feedback reflectivity are $r^2=0.99$ (solid line), $r^2=0.5$ (dashed line), and $r^2=0.1$ (dots). The light scattering loss $\alpha_s=5\ \mathrm{cm}^{-1}$.

will experience positive gain, in analogy to stimulated Brillouin scattering effect. Similar results are obtained if the input is an extraordinary (e) wave, and the stimulated scattering is an ordinary (o) wave.

B. Stimulated thermal scattering (STS)

Similarly, in the case of stimulated thermal scattering, the incident E_L and its scattered coherent noise E_S are described by

$$E_L(z)=E_L(0)e^{-(\alpha/2)z}, \tag{37a}$$

$$\frac{dE_S}{dz}=\gamma_T e^{\alpha z}E_S-\frac{\alpha}{2}E_S, \tag{37b}$$

$$\gamma_T=i\frac{n_0\omega^2}{k_{Sz}c^2}\left\{\frac{\alpha\dfrac{dn}{dT}\left(\dfrac{n_0 c}{8\pi}\right)|E_L|^2}{\rho c_p Dq^2}\frac{1}{1-i\Omega\tau_T}\right\},$$

$$=i\frac{\omega\alpha\left(\dfrac{dn}{dT}\right)I_L}{c\rho c_p Dq^2\cos\dfrac{\Theta}{2}}\frac{1+i\Omega\tau_T}{1+(\Omega\tau_T)^2}=g_T+i\kappa_T, \tag{38}$$

Note that

$$g_T=\mathrm{Re}\{\gamma_T\}=\frac{\omega\alpha\left(\dfrac{dn}{dT}\right)I_L}{c\rho c_p Dq^2\cos\dfrac{\Theta}{2}}\frac{-2\Omega\tau_T}{1+(\Omega\tau_T)^2}. \tag{39}$$

C. Maximum gain factors and material parameters

From Eqs. (36) and (39), note that both SOS and STS gains are maximum at $\Omega\tau=1$. In terms of the optical intensity, these maximum gains can be written as $g_R=G_r I_o$ and $g_T=G_T I_o$, respectively.

For SOS, we have $q=\sqrt{k_e^2+k_o^2-2k_ek_o\cos\Theta}$, and so

$$G_r=\frac{\omega\varepsilon_a^2}{8c^2n_on_eK_2q^2}. \tag{40}$$

For STS, $q=2k\sin(\Theta/2)$, and we have

$$G_T=\frac{\omega\dfrac{dn}{dT}\alpha}{2c\rho c_pDq^2\cos\dfrac{\Theta}{2}}=\frac{\lambda\dfrac{dn}{dT}\alpha}{16\pi\rho c_pD}\frac{1}{\sin^2\dfrac{\Theta}{2}\cos\dfrac{\Theta}{2}}, \tag{41}$$

where Θ is the crossing angle between E_1 and E_2. In general, the gain factors increases as the crossing angle Θ increases. For the SOS process, G_r is maximum at $\Theta=0$, i.e. forward SOS is the most-favored process. Furthermore, if we substitute $\varepsilon_a=n_e^2-n_o^2$, $q^2\sim(n_e-n_o)^2/\lambda^2$ into the above expression, we obtain

$$G_r\sim\frac{(n_e+n_o)^2\lambda}{n_\perp c}\left(\frac{1}{\eta K}\right). \tag{42}$$

This expression for G_r shows that it is *primarily dependent on the viscosity coefficient* η *and the elastic constant K*, and is essentially *independent of the dielectric anisotropy* ε_a.

For forward stimulated orientational scattering, the crossing angle $\Theta=0$ and the grating constant $\Lambda=\lambda/(n_e-n_o)$. Since the light wavelength $\lambda\approx0.5\,\mu$m, and the refractive indices of the NLC $E7$ are $n_o\approx1.54$ and $n_e\approx1.75$, the grating constant $\Lambda\approx2.5\,\mu$m. Using these values and the values for the elastic constant $K_2\approx3\times10^{-7}$ dyn, the dielectric anisotropy $\varepsilon_a=n_e^2-n_o^2\approx0.6$, the intensity gain factor $2G_R=1.4\times10^{-2}$ cm/W. The scattering loss coefficient of NLCs is about 20 dB/cm, or 4.6 cm^{-1}, so that we have $f(\alpha1)=0.95$, and the effective gain is $2G_{\text{eff}}=2G_rf(\alpha1)=1.3\times10^{-2}$ cm/W. For an interaction length (NLC film thickness) $d=200\,\mu$m, this gives a gain coefficient $2G_{\text{eff}}d=2.6\times10^{-4}\,\text{cm}^2/\text{W}$. In other words, the gain coefficient will be >1 for an input intensity of over $4\times10^3\,\text{W/cm}^2$, when the orientational fluctuation noise will gives rise to a stimulated emission of the orthogonally polarized Stokes waves. This threshold value is indeed in close agreement with results reported previously [7], and also with recent observations to be discussed in Sec. V.

For the thermal effect, the parameters of the liquid crystal are $\rho\approx1\,\text{g cm}^{-3}$, $c_p\approx2\,\text{J g}^{-1}\text{K}^{-1}$, $D\approx2\times10^{-3}\,\text{cm}^2\,\text{s}^{-1}$, and $dn/dT\approx10^{-3}\,\text{K}^{-1}$. The absorption is about $\alpha_a\approx20\,\text{cm}^{-1}$ (this value can be adjusted by the dopant dye concentration). For the experiment, $\lambda\approx0.5\,\mu$m, $\Theta=1°$ [this gives $\cos(\Theta/2)\approx1$ and $\sin^2(\Theta/2)\approx\Theta^2/4\approx(1.3\times10^4)^{-1}$]. From these parameters, we obtain the intensity gain factor $2G_T=1.3\times10^{-1}$ cm/W, which is an order of magnitude larger than $2G_{\text{eff}}$. Consequently the threshold optical intensity for observing STS is also about an order of magnitude lower. Again, this is in good agreement with the experimental observation of STS [8].

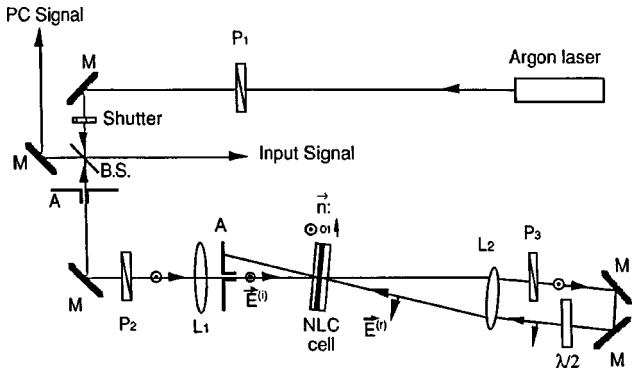

FIG. 6. Experimental setup for self-starting optical phase conjugation with stimulated orientational scattering effect. Polarizers $P2$ and $P3$ are parallel, lens L_1 has a focusing length $f_1=10$ cm, and lens L_2 has a focusing length $f_2=20$ cm.

V. EXPERIMENTAL RESULTS

Some preliminary experimental results for SOS, STS, and SSOPC have been reported previously [7,8]. Here we discuss mainly hitherto unreported results that further corroborate the theoretical formalism developed in the preceding sections.

A. Self-pumped phase conjugation with SOS effect

The experimental setup is shown in Fig. 6. The liquid crystal used is pure *E*-7 (EM Chemicals), which has a nematic-isotropic phase transition temperature $T_c=60.5\,°\text{C}$. The absorption of $E7$ at the laser wavelength (514.5 nm) is negligibly small. The experiment is conducted at room temperature that is far below T_c to further minimize any thermal indexing effect. The NLC cell is 200 μm thick and is planar aligned with the director axis of the NLC lying in the plane of the cell window. The cell is mounted on a rotator so that the director **n** can be varied from being parallel to perpendicular to the polarization of the incident optical **E** field.

Using this setup, but with the feedback beam blocked, we recently repeated the forward SOS experiment, using a tight focusing lens for the input, and a freshly made 200-μm-thick planar NLC cell. The focused spot diameter is about 30 μm. The incident laser is *e* polarized, and a polarizing beam splitter at the output end is used to separate the extraordinary (*e*) and ordinary (*o*) waves. Figure 7 summarizes the results obtained, showing the transmitted *e* wave and the generated *o* wave as a function of the input laser power. Above an input of 45 mW, corresponding to an estimated intensity of $\sim5\times10^3\,\text{W/cm}^2$, the stimulated scattering signal become clearly evident, as shown in the photographs accompanying Fig. 7. The threshold intensity obtained here is in good agreement with the value reported previously, and the theoretical estimate given in Sec. IV. Below threshold, both the transmitted *e* and *o*-wave noises are linearly dependent on the input power. Above threshold, the stimulated *o* wave grows dramatically, eventually surpassing the power of the transmitted *e* wave.

The simplicity of the experimental setup for observing stimulated *e*-*o* wave scatterings allows one to make a quantitative comparison between theory and experimental results, especially in the low signal regime when the signal wave

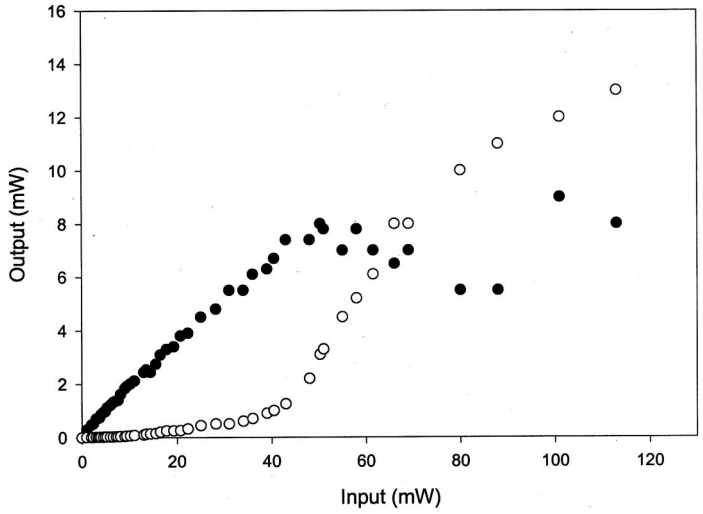

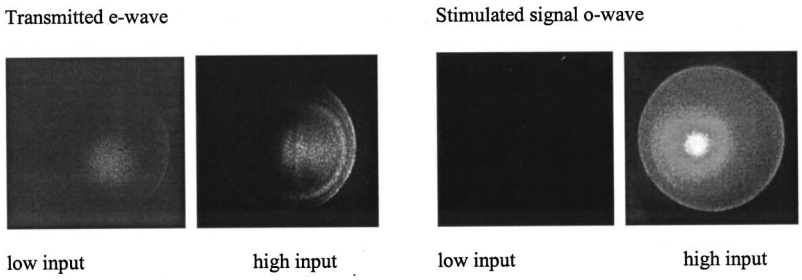

FIG. 7. Dependence of the transmitted *e* wave (dots) and the stimulated *o*-wave power (circles) on the input *e*-wave power. Insets are photographs of the *e* and *o*-wave outputs below and above the stimulated scattering threshold. The laser spot diameter is 30 μm.

grows exponentially with the input light intensity. Figures 8(a) and 8(b) shows the curve fitting done for the respective stimulated scattering results obtained in a previous study [7]. From these results, we deduce the gain parameters to be $2G_R(o\text{-}e)=2.4\times10^{-2}$ cm/W and $2G_R(e\text{-}o)=1.5\times10^{-2}$ cm/W. This compare very favorably with the theoretical estimate made in Sec. IV for a gain parameter on the order of $2G_R=1.4\times10^{-2}$ cm/W. The deviation between theory and experiment is most likely due to losses (scattering and reflection) and actual values of the liquid crystal parameters, and some simplifying approximations (plane wave, one elastic constant etc.) used in the theory.

Returning now to the SSOPC experiment, the feedback beam E_2 is obtained by reflection from the external mirrors. The reflectivity is 0.55, and the reflected beam makes an angle of 45° with the incident beam. We have investigated the dependence of the SSOPC processes on the initial orientation of the incident field polarization vector with respect to the director axis of the NLC. In the first configuration, the incident wave is either a pure *o* wave or a pure *e* wave; a half-wave plate is used to rotate the polarization of the reflection beam $\mathbf{E}_2$ by 90° to make it orthogonal to that of $\mathbf{E}_1$. In the second configuration, the director *n* of the NLC cell is rotated to make an angle of 45° with the polarization direction of E_1, and the half-wave plate behind the cell is removed.

For both setups, SPC signals become clearly visible when the incident laser power exceeds the threshold value, appearing in the far field as a bright spot in contrast to the fuzzy appearance of the noise background. As previously reported [7], the phase-conjugated signal is spatially of the same quality as the input laser beam, and has approximately the same divergence, in spite of the aberration imparted by the input lens and other optics. A typical time evolution of the SSOPC signal is shown in Fig. 9(a). When the incident light intensity is below the threshold, the small noise signal has a square-pulse shape with a flat top (the bottom curve), similar to the incident square pulse. Above the threshold, the signal increases dramatically (the top curves). The buildup time of the signal shortens as the pump intensity I_o is raised.

The dependence of signal intensity on the incident beam intensity at steady state are shown in Figs. 9(b) and 9(c) for both types of experimental setup. From Fig. 9(b), the observed threshold intensity is estimated to be on the order of 5 KW/cm^2 (500 mW in a focused spot diameter of 100 μm), which is in good agreement with the theoretical expectations: [c.f. Fig. 4(b)] $r^2=0.5$ and $\alpha=5$ cm^{-1}. In general, the second setup, in which the incident laser polarization makes an angle of 45° with the LC director axis, exhibits a lower threshold. This is expected as this configuration provides a much stronger initial seed signal wave.

B. Self-pumped phase conjugation with STS effect

The liquid crystal used is BDH K15 (Pentyl-Cyano-Biphenyl 5CB from EM Chemicals) doped 0.5% by weight with a dichroic dye D16 (Em Chemicals) to enhance the light absorption and the thermal effect. The planar aligned sample is made by sandwiching the liquid crystal between two prisms with rubbed polymer-coated surfaces. The film thickness is 150 μm and the sample is put into a temperature controlled cell. To avoid overheating the NLC, the laser pulse duration is limited to $<$10 ms. The laser is linearly polarized, with the polarization vector ($\mathbf{E}_1$ and $\mathbf{E}_2$) parallel

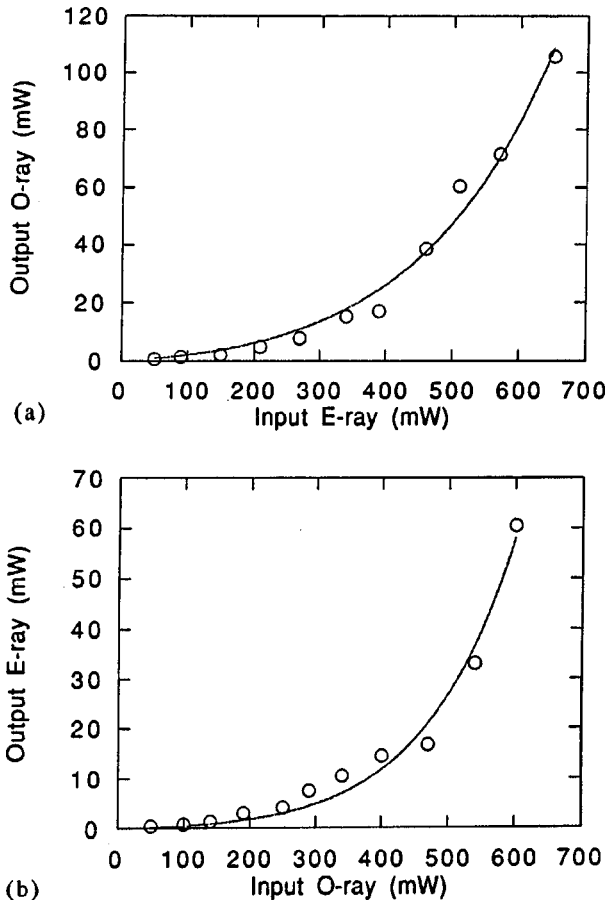

FIG. 8. Dependence of the observed stimulated scattering signals (circles) on the input light power, and theoretical fitting curves (solid lines). (a) *e*- to *o*-wave scattering. (b) *o*- to *e*-wave scattering. The laser spot diameter is 50 μm.

to the director axis **n** of the liquid crystal, so that the index grating is associated with the temperature-dependent extraordinary refractive index $n_e(T)$. At room temperature, n_e of 5 CB is 1.68, whereas the prisms have a refractive index of 1.73.

A ring-cavity configuration as depicted in Fig. 10 is employed for this experiment. The laser is obliquely incident upon the cell, as shown in Fig. 10, so that the effective interaction length within the liquid crystal is about 1 mm. As a result of reflection loss at the glass-liquid crystal interface and scattering and absorption loss in the liquid crystal, only 5% of the incident beam is transmitted. The transmitted beam is recollimated, and focused back into the cell, making an angle $\theta \approx 1°$ with the incident beam. The spot diameter of the input laser at the liquid crystal is 0.5 mm, whereas the reflected beam spot size is approximately five times smaller, i.e., $2\omega_o = 0.1$ mm. Therefore, the intensities of the input and reflected beams in the overlap region are roughly equal. A beam splitter placed in the path of the incident and the reflected beam is used to monitor the phase-conjugated and reflected signals simultaneously.

A phase-conjugated signal, which propagates along the reverse direction of $\mathbf{E}_1$, becomes visible when the input laser power is about 400 mW and the cell temperature is maintained within 5 °C below T_c—the phase-transition temperature of the nematic liquid crystal. For 5CB, $T_c = 35$ °C. The phase-conjugated signal is spatially of the same quality as the input beam, and has approximately the same divergence. On the other hand, the reflected signal is considerably defocused by the input optics and propagates along different di-

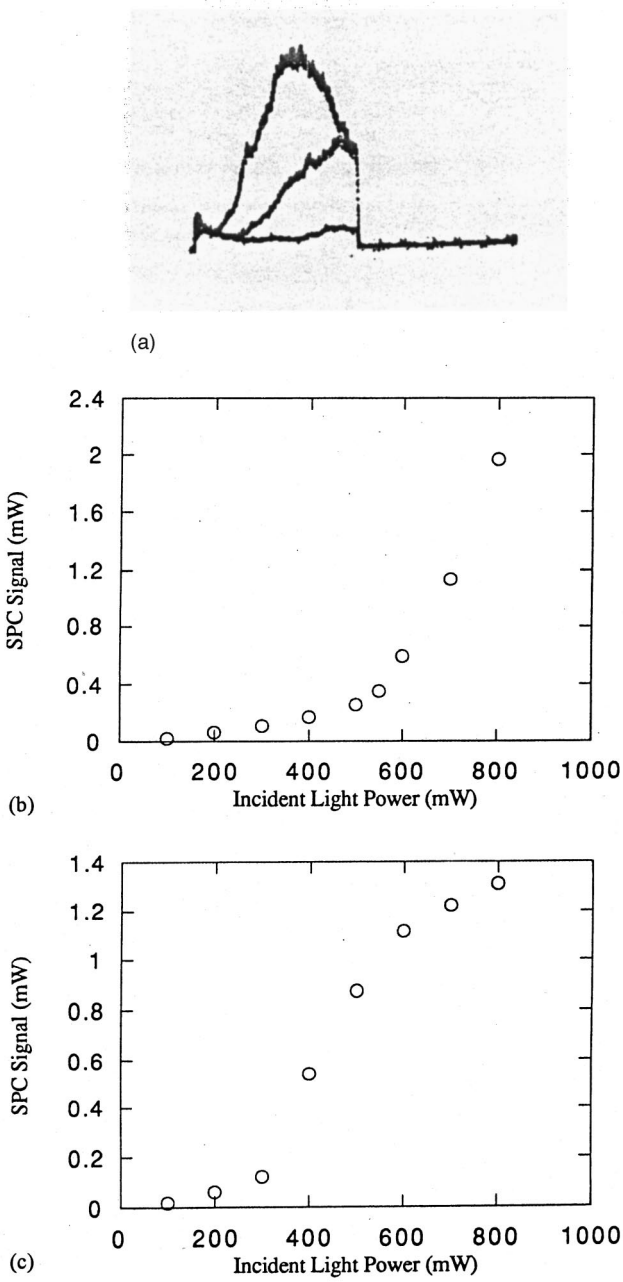

FIG. 9. (a) Oscilloscope record of self-pumped optical phase conjugation signals generated by the second kind of setup at different incident beam powers. Upper curve: $P = 560$ mW. Middle curve: $P = 400$ mW. Lower curve: $P = 300$ mW. The pulse width is 50 ms. (b) Power of the self-pumped phase conjugation signal as a function of the incident pump power with the first kind of setup; the incident beam is an *o* wave and the reflection beam is an *o* wave. The peak phase conjugation efficiency (at an input power of 800 mW) is estimated to be 2.5%. (c) Results obtained with the second kind of setup. The polarization direction of the incident beam and the reflection are parallel, while the director of the NLC cell is placed at a 45° angle from them. The peak phase conjugation efficiency is estimated to be 1.8% (at an input power of 800 mW).

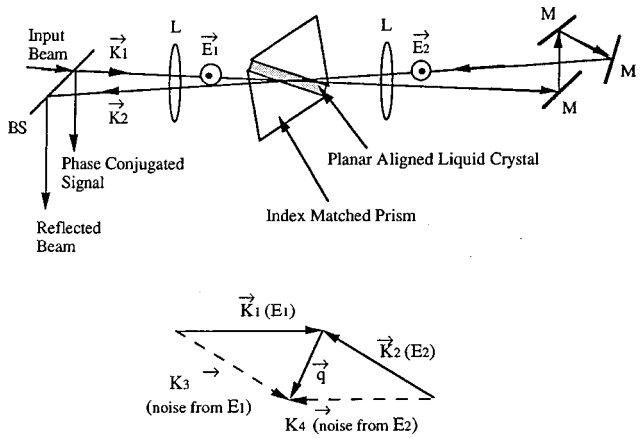

FIG. 10. Experimental setup and wave-vector matching diagram for self-pumped optical phase conjugation with stimulated thermal scattering effect.

rections as θ is varied.

1. Dependence of the SPC signal on the pump intensity

Figure 11 shows the dependence of the phase-conjugated signal on the incident beam power, while the temperature of the NLC sample is fixed. When the incident power is below 600 mW, only scattering noise is detected in the direction of $\mathbf{k}_4$; the noise is linearly dependent on the incident power, just as the reflected light from the sample. Above a threshold of 600 mW, a dramatic increase in the phase-conjugated signal, corresponding to the onset of stimulated scattering and self-oscillation, is observed. The threshold intensity value is estimated to be 240 W/cm^2 (600 mW in a spot diameter of 0.5 mm), in good agreement with the theoretical estimate made in Sec. IV.

2. Dependence of the SPC signal on temperature

The dependence of the phase-conjugated signal power on the input beam for different cell temperatures is shown in Fig. 12. We can see that the closer the cell temperature is to

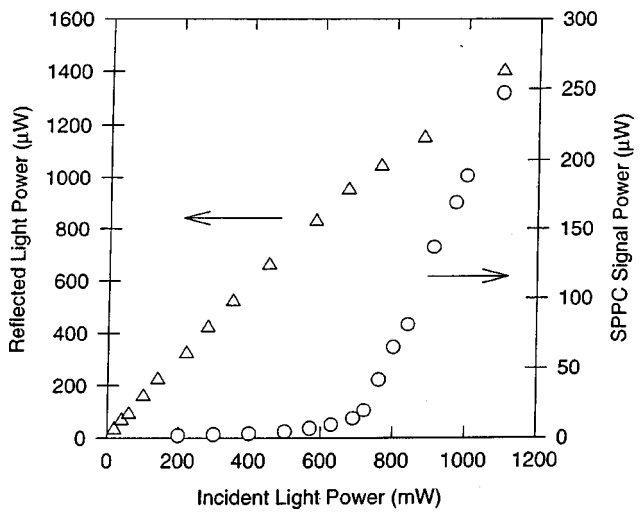

FIG. 11. Power of the reflected light (triangles) and the optical phase conjugation signal (circles) as a function of the incident light power.

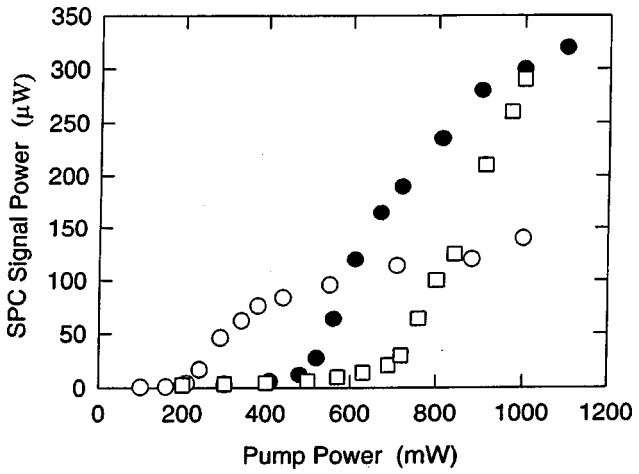

FIG. 12. Influence of the temperature on self-pumped optical phase conjugation signal. $T_c - T = 13\,^\circ$C (squares); $T_c - T = 8\,^\circ$C (dots); $T_c - T = 2.5\,^\circ$C (circles).

T_c, the lower the threshold is for SSOPC. This is due mainly to the fact that the gain coefficient is proportional to the index gradient dn/dT, which increases as the temperature approaches T_c. A further measurement of the phase-conjugated signal intensity as a function of the NLC cell temperature was conducted when the input laser power was kept as a constant, and the result is shown in Fig. 13. Again, because of the increase in the magnitude of the thermal-index gradient at temperature $T \rightarrow T_c$, with a larger coupling coefficient γ, the SSOPC signal increases as we approach T_c.

3. Dynamics of the SPC signal

The SSOPC signal should build up in accordance with the dynamics of the laser-induced temperature and refractive index changes. The stronger the intensity, or the nearer the temperature is to T_c, the larger the induced index modulation δn and thus the coupling coefficient γ. We therefore expect the oscillation of the phase-conjugated signal to build up sooner. Figure 14 shows the observed buildup time for

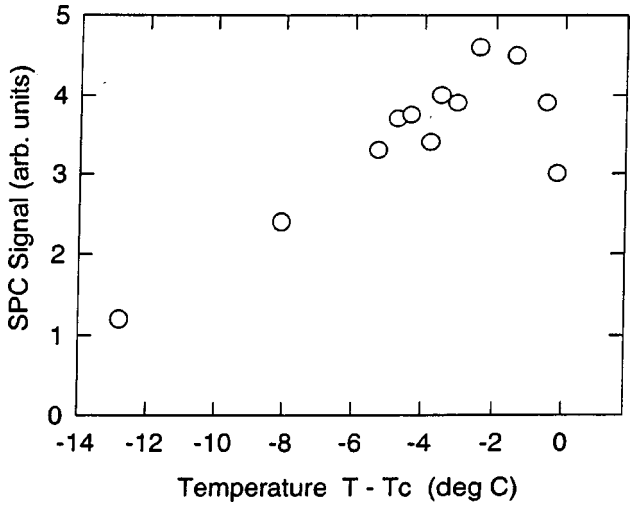

FIG. 13. Dependence of the optical phase-conjugated signal power on temperature at $P_m = 55$ mW. The peak SPC reflectivity is about 2%.

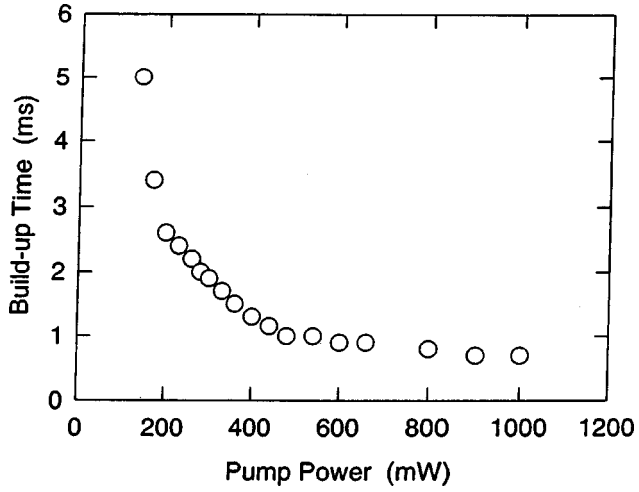

FIG. 14. Buildup time of the optical phase-conjugated signal as a function of the incident light power $T_c - T = 3.6\,^{\circ}\mathrm{C}$.

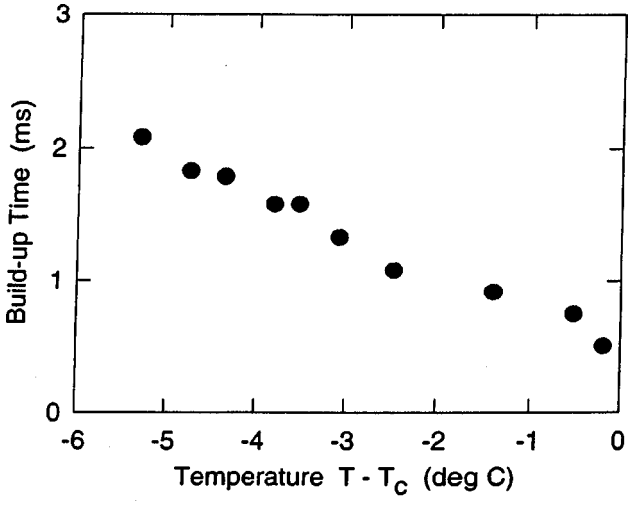

FIG. 15. Buildup time of the optical phase-conjugated signal as a function of the ambient temperature. $P_{\mathrm{in}} = 500\,\mathrm{mW}$.

input laser powers ranging from 200 to 600 mW, showing that it drops off considerably as the input laser power is increased. Above a power of 500 mW, a submillisecond buildup time is achieved. Similar results are obtained if the laser power is kept constant, but the liquid crystal cell temperature is increased toward T_c. The results plotted in Fig. 15 show that the buildup time decreases to a submillisecond value as the temperature approaches T_c. Besides generating a larger refractive index change, an increase in the temperature of the sample also causes a higher scattering noise level η_{ss}. It was demonstrated [1,15] in theories and experiments that the magnitude of this coherent noise affects the buildup time in a similar fashion, i.e., larger initial noise sources ($\mathbf{E}_3$ and $\mathbf{E}_4$) will shorten the buildup time. Therefore, the observed results in Fig. 15 are attributed to the higher refractive index change δn as well as the noise level η_{ss}.

VI. FURTHER REMARKS AND CONCLUSION

We have presented a quantitative theoretical and experimental study of self-starting optical phase conjugation in nematic liquid crystals using stimulated orientational or thermal scattering effects. Both SOS and STS are found to be quite efficient means of generating SSOPC. Since the birefringence and large thermal index coefficients of a nematic liquid crystal hold throughout the UV-infrared spectrum, these SOS, STS, and SSOPC processes are possible at other laser wavelengths besides the visible one used in this study. This is clearly an advantage over the limited operational bandwidth of electro-optic liquid crystal light valves, where the phase conjugation signal originates from the absorption of light at a semiconducting surface [16,17]. It is important to point out again that in SOS, there is very little variation of the basic parameters such as gain and oscillation thresholds on the laser wavelength. On the other hand, STS does require some absorption at the wavelength of interest, which could come about from the liquid crystal's natural absorption or some appropriate dopant. We are currently studying these nonlinear optical processes with the use of 1.3–1.5-μm lasers, as well as developing a complete theory that could account for pump depletion that will occur at high conversion efficiency.

ACKNOWLEDGMENTS

We gratefully acknowledge technical assistance by M. Y. Shih, P. H. Chen, A. Shishido, and technical discussions with N. V. Tabiryan. This work was supported by the Army Research Office, the Air Force Research Laboratory (Kirtland Air Force Base), and the National Science Foundation.

[1] B. Ya. Zeldovich, N. F. Pilipetsky, and V. V. Shkunov, *Principles of Phase Conjugation*, Springer Series in Optical Sciences Vol. 42. (Springer-Verlag, Berlin, 1985). For the transient SSOPC effect in NLC with high power ruby laser pulses, see, for example, B. Ya. Zeldovich, S. K. Merzlinkin, N. F. Pilipetskii, and A. V. Sukhov, Pis'ma Zh. Eksp. Teor. Fiz. 41, 418 (1985) [JETP Lett. **41**, 514 (1985)].

[2] K. D. Ridley and A. M. Scott, Opt. Commun. **76**, 406 (1990); Int. J. Nonlinear Opt. Phys. **1**, 563 (1992).

[3] J. Feinberg, Opt. Lett. **7**, 486 (1982).

[4] J. O. White, M. Cronin-Golomb, B. Fischer, and A. Yariv, Appl. Phys. Lett. **40**, 450 (1982); M. Cronin-Golomb, B. Fisher, J. O. White, and A. Yariv, IEEE J. Quantum Electron. **QE20**, 12 (1984); Appl. Phys. Lett. **42**, 919 (1983).

[5] C. J. Gaeta, J. F. Lam, and R. C. Lind, Opt. Lett. **14**, 245 (1989).

[6] M. Vallet, M. Pinard, and G. Grynberg, Opt. Lett. **16**, 1071 (1991).

[7] I. C. Khoo and Yu Liang, Opt. Lett. **20**, 130 (1995).

[8] I. C. Khoo, H. Li, and Y. Liang, Opt. Lett. **18**, 1490 (1993).

[9] O. L. Antipov, Opt. Commun. **103**, 499 (1990); O. L. Antipov, N. A. Dvoryaninov, and V. Sheshkauskas, Pis'ma Zh. Eksp. Teor. Fiz. **53**, 586 (1991) [JETP Lett. **53**, 610 (1991)].

[10] F. Sanchez, P. H. Kayoun, and J. P. Huignard, J. Appl. Phys. **64**, 26 (1988).

[11] I. C. Khoo, P. Y. Yan, G. M. Finn, T. H. Liu, and R. R.

Michael, J. Opt. Soc. Am. B **5**, 202 (1988).
[12] I. C. Khoo and S. T. Wu, *Optics and Nonlinear Optics of Liquid Crystals* (World Scientific, Singapore, 1993); I. C. Khoo, *Liquid Crystals: Physical Properties and Nonlinear Optical Phenomena* (Wiley-Interscience, New York, 1995).
[13] I. C. Khoo, Phys. Rev. Lett. **64**, 2273 (1990).
[14] N. V. Tabiryan, B. Ya. Zel'dovich, and A. V. Sukhov, Mol. Cryst. Liq. Cryst. **136**, 1 (1986).
[15] A. V. Mamaev and A. A. Zozulya, Opt. Commun. **79**, 373 (1990); I. C. Khoo, N. Beldyugina, Hong Li, A. V. Mamaev, and V. V. Shkunov, Opt. Lett. **18**, 473 (1993).
[16] O. V. Garibyan, I. N. Kompanets, A. V. Parfyonov, N. F. Pilipetskii, V. V. Shkunov, A. N. Sudarkin, A. V. Sukhov, N. V. Tabiryan, A. A. Vasiliev, and B. Ya. Zel'dovich, Opt. Commun. **38**, 67 (1981).
[17] A. Brignon, I. Bongrand, B. Loiseaux, and J.-P. Huignard, Opt. Lett. **22**, 1855 (1997).